Effects of Initial Structure on the Deformation Behavior of PP Hollow Fiber in Continuous Drawing

MOO SEOK LEE, SANG YONG KIM

Department of Fiber & Polymer Science, College of Engineering, Seoul National University, San 56-1, Shinlim-Dong, Kwanak-Ku, Seoul 151-742, South Korea

Received 9 April 2000; accepted 17 May 2000

ABSTRACT: The effects of the microcrystalline structure of undrawn fibers on the rheological behavior in the process of the polypropylene (PP) hollow fiber formation system were studied by a simple model describing the continuous drawing process. The predicted and observed drawing behaviors were explained in view of a simple approach based on the concept of strain-rate sensitivity and strain-hardening parameters. Various parametric studies showing the interactive nature of the strain-rate sensitivity and strain-hardening parameters on the drawing behavior were also numerically performed. Strain-rate sensitivity affects mainly the intensity of the neck, and strain hardening has more effects on the position of the inflection point in continuous drawing. Details of the necking mechanism in the drawing process were studied by observing the deformation behavior of the specimens with different initial microcrystalline structures. The distinctive initial structure of undrawn PP hollow fibers can be formed by controlling the quenching condition in melt spinning. It was shown that the water-quenched PP fiber exhibited an unstable smectic form, whereas the stable monoclinic phase was observed for the fiber prepared without quenching by forced convection. The experimental results of the drawing behavior indicated that the strain-rate sensitivity of the fiber with a smectic form was larger than that with the monoclinic form. It was also shown that the hollowness was affected by the quenching condition in melt spinning and the deformation behavior in the drawing process. © 2001 John Wiley & Sons, Inc. J Appl Polym Sci 81: 2170–2182, 2001

Key words: hollow fiber; strain-rate sensitivity; strain hardening; polypropylene; necking

INTRODUCTION

The deformation mechanism of polymers has been a subject of considerable interest from both theoretical and practical points of view. Among the many stretching processes, the continuous drawing of melt-spun fiber is an important step in the fiber-forming process, and optimization of the drawing process to achieve the desired final properties has been an essential part of process-development studies.

The development of plastic instabilities during the large deformation of solid polymers is a significant characteristic to be considered in the drawing of solid polymers. Particularly, the neck geometry and its propagation have been the major scope of a number of studies.[1–4] Among the many approaches for this subject, Coates and Ward[1] accounted for the necking phenomenon in terms of strain hardening and strain-rate sensitivity, and many other workers[2–4] considered these parameters as a tool for the analysis of the

Correspondence to: M. S. Lee (nostein@dreamwiz.com).

Journal of Applied Polymer Science, Vol. 81, 2170–2182 (2001)

neck geometry in the drawing of solid polymers. The relationship of neck geometry and neck propagation to the true stress, true strain, and true strain-rate surface was discussed by Coates et al.[1,5] Nazarenko et al.[2] also studied the effect of temperature and pressure on necking behavior, following the concept of strain hardening and the strain-rate sensitivity effect. They explained the effects of the pressure and temperature on strain hardening and the strain-rate sensitivity parameter of polycarbonate by experimental and numerical methods. The structural analysis on the necking of polyethylene was performed by Gaucher-Miri et al.[3] with the aid of X-ray diffraction, and in this work, strain hardening and strain-rate sensitivity were considered as factors of the neck geometry of polyethylene. However, such structural or numerical analyses have been concentrated on tensile drawing at a constant rate of elongation or creep tests. On the other hand, little work has been done in relation to the deformation behavior in the continuous drawing process in spite of its industrial significance.

In continuous drawing, machine variables such as the applied draw ratio and drawing velocity do not have a unique correlation with the final fiber properties,[6] since the fiber elements actually go through the various states of the stress–strain–strain rate along the drawing path for given machine variables. Thus, local variables at every position of the drawing path must be investigated to understand the deformation behavior and to control the final properties of drawn fibers. Therefore, there is a need to develop a quantitative description of the initiation, stabilization, and propagation of the neck and the profiles of various local variables in the continuous drawing of solid polymers. In our previous article,[7] the realistic strain localization in continuous drawing was calculated using a constitutive equation that can describe the inherent viscoplastic behavior of solid polymers.

In general, a fiber-formation system consists of melt-spinning and drawing processes, and the structure developed during melt spinning determines the rheological behavior of the material in subsequent drawing.[8] Thus, the effects of spinning conditions on the subsequent drawing behavior can be explained by the strain hardening and strain sensitivity of undrawn filaments with different initial structures. Particularly, study of the drawing behavior according to the different initial microcrystalline structures was necessary for polypropylene (PP) hollow fibers that can be used for special end uses such as membranes.[9,10] The PP hollow fibers have a microporous structure by melt-spinning and cold-stretching methods.[9] Therefore, a detailed prediction and the control of the drawing behavior with respect to the initial structure are essential to obtain the optimum properties of PP hollow fibers for final use. In this article, a numerical analysis was performed to determine the relation between the rheological property of an undrawn filament and the significant drawing parameters in continuous drawing: drawing force, intensity of strain localization, and position of the inflection point. Experiments showed that undrawn PP hollow fibers, which were produced under different quenching conditions during melt spinning, have two distinctive microcrystalline structures, and the initial structure affects the neck geometry. This result is discussed in terms of rheological properties based on the parametric studies. The hollowness, which is the main characteristic of the hollow fiber, was also observed from the experiments.

EXPERIMENTAL

Sample Preparation

The material used in this work was isotactic PP with molecular weights of M_n = 36,900 and M_w = 211,000. To prepare undrawn hollow fibers, PP was melt-spun, through a spinneret that consists of three segmented arcs, with a laboratory-scale melt-spinning system. The melt-spinning apparatus consisted of an extruder, a quench box, and a take-up device. To produce the specimens with different structures, the filaments were separately spun without any forced cooling system and with a quenching system. The molten polymer was quenched by a water bath of 20°C, which was set at the position of 11.6 cm below the spinneret. The continuous inflow and outflow of water prevented a temperature change of the water bath by heat transfer from the hot molten polymers.

Drawing

The as-spun filaments were drawn continuously with a drawing apparatus that consisted of a feed roll, temperature-controlled water bath, take-up roll, and tensiometer. To investigate the neck profile, the part of the filament containing the neck was cut from the filament in the drawing line and its

outer diameter profile was obtained by image analysis. The specimens with and without quenching were drawn at several drawing temperatures.

Characterization

Wide-angle X-ray diffractograms of as-spun filaments were obtained with a General Area Detector Diffraction System supplied by Bruker Axs. It offered a real-time display of the visible diffraction image by advanced two-dimensional detector technology. WAXS intensity curves of equatorial scans were obtained at angles (2θ) varying from 0° to 30°. Differential scanning calorimetry was done on a Perkin–Elmer DSC 7 over the temperature range from −30 to 200°C. The thermograms were obtained using samples of about 5 mg at a heating rate of 20°C/min. The viscoelastic behavior of undrawn PP filaments was observed using a Rheometric Scientific DMTA MK II. Measurement was performed at a constant frequency of 10 Hz and a heating rate of 2°C/min, over the temperature range from −50 to 150°C. To estimate the relative quantity of the hollow portion of the fiber, hollowness, defined as the ratio of area of the hollow portion to the total cross-sectional area, was measured using an image-analysis system with a built-in microscope.

MODELING OF CONTINUOUS DRAWING

Most industrial drawing processes of films and fibers are continuous operations between two rolls with different velocities. To simulate the deformation behavior of solid polymers in continuous drawing, a simple drawing system was considered in this work: The filaments were drawn continuously in an isothermal bath that is controlled to maintain a constant temperature. Some assumptions for the formulation describing this drawing system are as follows:

First, a constant drawing force was assumed because the inertia and drag force can be negligible compared with the rheological force.[8,11,12] The temperature of the filaments in the deformation zone, that is, in a water bath, was assumed to be kept at ambient water temperature. A plug flow was assumed, as employed in some studies,[1,13] to develop a one-dimensional formula. Continuous drawing can be considered to be steady state, and incompressibility of the filaments was assumed.

The following governing equations, describing continuous drawing, can be obtained by considering the conservation of the mass and momentum with a rheological equation of solid polymers:

$$\rho A v = W = \text{const.} \tag{1}$$

$$F = \sigma A = \text{const.} \tag{2}$$

$$\sigma = k[1 - \exp(-\omega\varepsilon)]\exp(h\varepsilon^2)(\dot{\varepsilon}/\dot{\varepsilon}_0)^m \tag{3}$$

where A, v, and F denote the area, axial velocity, and tensile force, respectively; σ is the true stress; ε, the true strain; and $\dot{\varepsilon}$, the true strain rate of the filament at a distance, x, from the feed roll; $\dot{\varepsilon}_0$, ρ, and W, the reference strain rate (conventionally equal to 1 s^{-1}), density, and mass flow rate, respectively; and k, h, ω, and m, rheological coefficients at a given temperature, denoting the scaling factor, strain-hardening factor, viscoelastic coefficient, and strain-rate sensitivity coefficient, respectively. By combining some definitions of local variables as a function of a position, x, and the above equations, one can obtain

$$x = \frac{v_0}{\dot{\varepsilon}_0}\left(\frac{k}{\sigma_0}\right)^{1/m}\int_0^{\varepsilon}\exp(\varepsilon)[\exp(h\varepsilon^2 - \varepsilon) - \exp(h\varepsilon^2 - (\omega+1)\varepsilon)]^{1/m}\,d\varepsilon \tag{4}$$

where v_0 and σ_0 are the feed roll velocity and the initial true stress, respectively. More details on the above equations were given in a previous article.[7]

Equation (4), with boundary conditions, gives information on the basic relation of deformation kinetics in continuous drawing. The plot of x versus ε can be obtained and it is possible to calculate some other variables such as σ, ε, $\dot{\varepsilon}$, v, and A from this relation. To obtain the distribution of the local true strain, ε, along the drawing line, the interval of ε from zero to a maximum value, ε_L, which is defined as ln DR (DR is an applied draw ratio), must be finely sectioned into small elements. For each element, numerical integration was performed. Because the material coefficients in the equation determine the range of DR at which the realistic profiles of drawing variables can be calculated, the proper values of coefficients must be selected for the successful simulation of a given drawing system. The material coefficients were chosen as listed in Table I for investigation of parameter sensitivity.

RESULTS AND DISCUSSION

Strain Localization

Employing the concepts of strain-rate sensitivity and strain hardening, the neck and strain localization of solid polymers during stretching can be analyzed. The strain-rate sensitivity parameter, *SRS*, and the strain-hardening parameter, *SH*, in this approach are defined as follows[2,3]:

$$SRS = \left(\frac{\partial \ln \sigma}{\partial \ln \dot{\varepsilon}}\right)_{\varepsilon} \tag{5}$$

$$SH = \left(\frac{\partial \ln \sigma}{\partial \varepsilon}\right)_{\dot{\varepsilon}} \tag{6}$$

We can express the Considère construction, which is usually used as an instability criterion for a polymer in terms of the strain-hardening parameter, as follows:

Case 1)

$$\left(\frac{\partial \ln \sigma}{\partial \varepsilon}\right)_{\dot{\varepsilon}} > 1 : \text{uniform extension without neck}$$

Case 2)

$$\left(\frac{\partial \ln \sigma}{\partial \varepsilon}\right)_{\dot{\varepsilon}} = 1 \text{ at one point : neck}$$

Case 3)

$$\left(\frac{\partial \ln \sigma}{\partial \varepsilon}\right)_{\dot{\varepsilon}} = 1 \quad \begin{matrix}\text{at two points : neck} \\ \text{and cold drawing}\end{matrix}$$

By applying the above criteria to the constitutive equation used in the simulation of continuous drawing, the leading factor for necking in the calculation, which will be presented later, can be understood:

$$SH = \left(\frac{\partial \ln \sigma}{\partial \varepsilon}\right)_{\dot{\varepsilon}} = \frac{\omega \exp(-\omega\varepsilon)}{1 - \exp(-\omega\varepsilon)} + 2h\varepsilon = 1 \tag{7}$$

Strain hardening, as a function of the true strain in the above equation, is shown in Figure 1 for the given material coefficients, h and ω, assigned in the calculation of continuous drawing. This result gives information that the material under consideration conforms to Case 3 in the Considère construction, that is, neck and cold drawing, since two points of $SH = 1$ appear in the plot. Nazarenko et al.[2] obtained the plot of SH versus ε from the data of the tensile test, and they illustrated neck and cold drawing from this plot. In Figure 1, the strain-hardening parameter decreases with increasing strain in the lower strain region. When the first point of $SH = 1$ appears, the deformation becomes unstable and the neck occurs in the specimen. The neck makes the filament thinner until it stabilizes by strain-hardening effects. When the hardening of materials is fully developed, $SH = 1$ is attained again and subsequent uniform cold drawing begins. Thus, if appropriate basic equations for continuous drawing are established with this constitutive equation, the neck profiles will be described without other special assumptions.

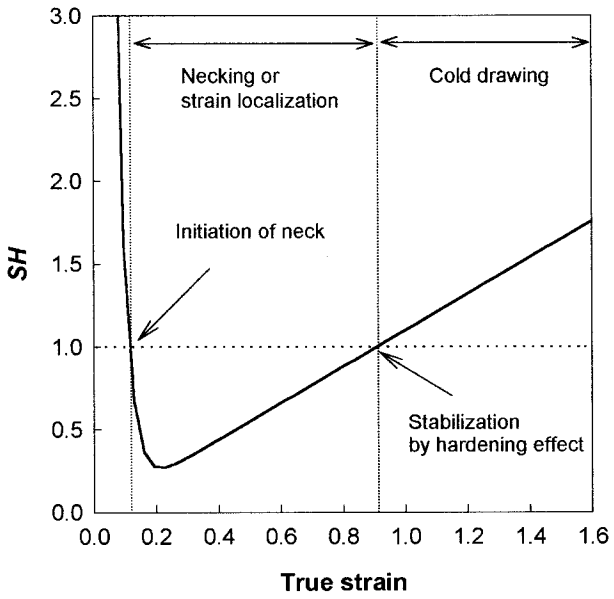

Figure 1 Variation of the strain-hardening parameter as a function of true strain: (dashed line) stability criterion, that is, Considère construction.

The calculated diameter profile is presented in Figure 2 with the strain-hardening parameter along the drawing line to indicate that the strain localization and subsequent cold drawing are due to the material characteristics. The criterion using the strain-hardening parameter makes it possible to provide a schematic regime for continuous drawing: initial elastic region, strain-localization region, and strain-hardening region. Before the position of the first point where $SH = 1$, the deformation of the filament will show linear elastic behavior and this deformation may be recoverable after drawing. In region II in Figure 2,

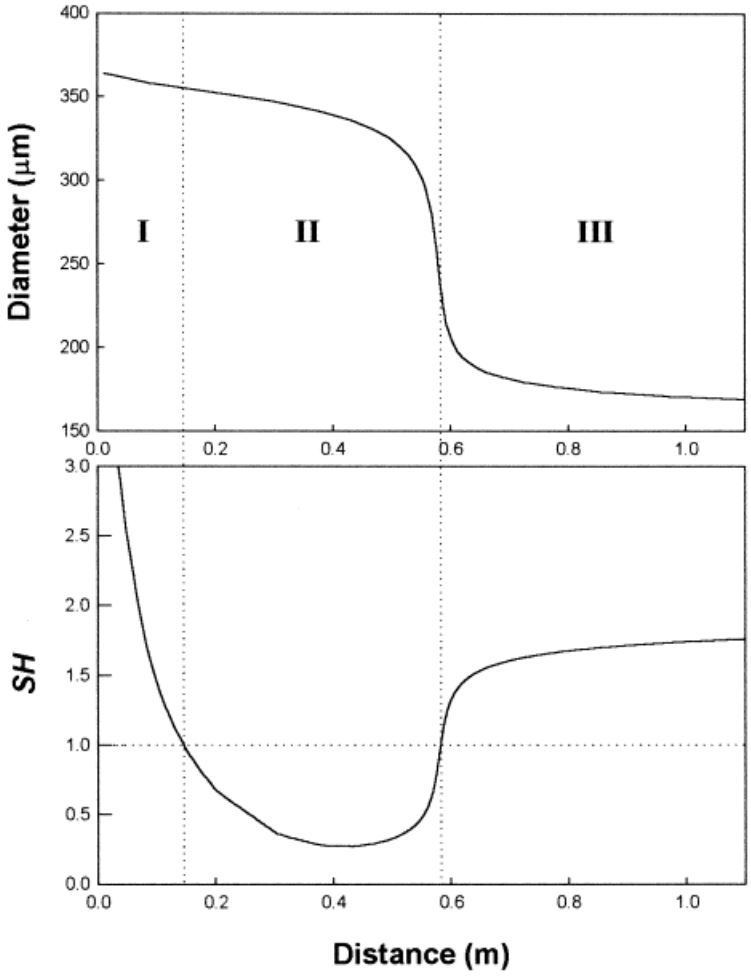

Figure 2 Regions along the drawing line divided by drawing characteristics: (I) initial recoverable elastic deformation region; (II) yield and strain-localization region; (III) strain-hardening region).

yield and strain localization occur, so that most of the strain given by the applied draw ratio is achieved in this region. After the second position where $SH = 1$, the filaments deform slightly under high stress because of the strain-hardening effect, and major structural development may occur in this region. The optimum process condition can be obtained by controlling the deformation history because the drawing condition and the properties of the undrawn material can affect the relative portion of each region.

The overall characteristics of deformation kinetics are shown in Figure 3. The various local variables in continuous drawing were calculated under typical conditions employed in the actual drawing experiments. The strain localization along the drawing line is described in this figure, and it can be found that the true strain rate has a maximum at the region of strain localization. The description of strain localization in this simulation is possible because the proper constitutive equation of viscoplastic polymers is used and it can be incorporated into the numerical scheme without any critical problem. The constant drawing force along the drawing line can also be calculated as shown in Figure 3. The drawing force is a very important factor in continuous drawing but usually unknown in an actual drawing system. The local true stress shows an abrupt increase near the position of the strain localization due to the reduction in area.

Material Parameter Sensitivity

The effects of material properties on the drawing behavior in continuous drawing were investi-

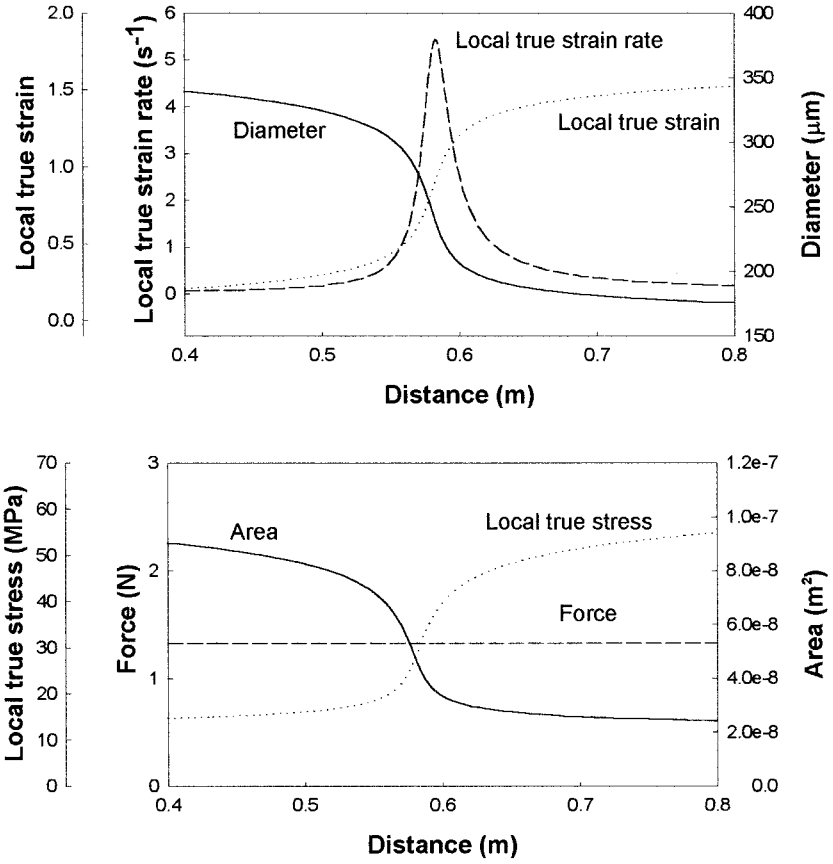

Figure 3 Various profiles of calculated local variables along the drawing line.

gated by choosing the m and h in the constitutive equation as a measure of strain-rate sensitivity and strain-hardening effects. Values of the material coefficients, m and h, used in these parametric studies were chosen from the range where the convergent profiles of local variables can be obtained, and they are listed in Table I.

The effects of the strain-rate sensitivity parameter, as defined in eq. (5), on the drawing behavior in continuous drawing can be investigated in terms of the strain-rate sensitivity coefficient, m, in the constitutive equation. The meaning of this parameter can be explained from the phenomenological standpoint by considering the two extremes: The ideal Hookean material shows complete dependence on the strain, whereas the Newtonian fluid is insensitive to the strain but is a function of only the strain rate. In other words, the material that is more sensitive to the strain rate than to the strain is expected to show a more fluidlike behavior.

Table I Rheological Parameters of PP Used for Parametric Study

k (MPa)	h	m	ω
40	0.54	0.03	33
	0.55	0.04	
	0.56	0.05	
	0.57	0.06	

The evolution of the diameter along the drawing line at various m is illustrated in Figure 4. Increasing the strain-rate sensitivity causes the inflection point to slightly shift to the left and produces a longer region of strain localization. It can also be found that the model material with the smallest value of m shows very sharp plastic instability. More insight into strain localization may be provided by Figure 5, which shows the true strain-rate profile as a function of the true strain with various m. The maximum strain rate decreases as m increases. Consequently, the sample with a larger m may show a more homogeneous deformation in continuous drawing.

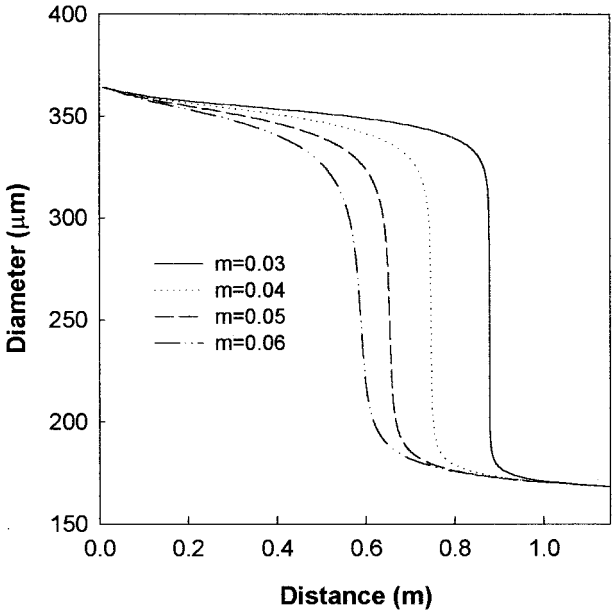

Figure 4 Effect of strain-rate sensitivity on the diameter profiles in continuous drawing.

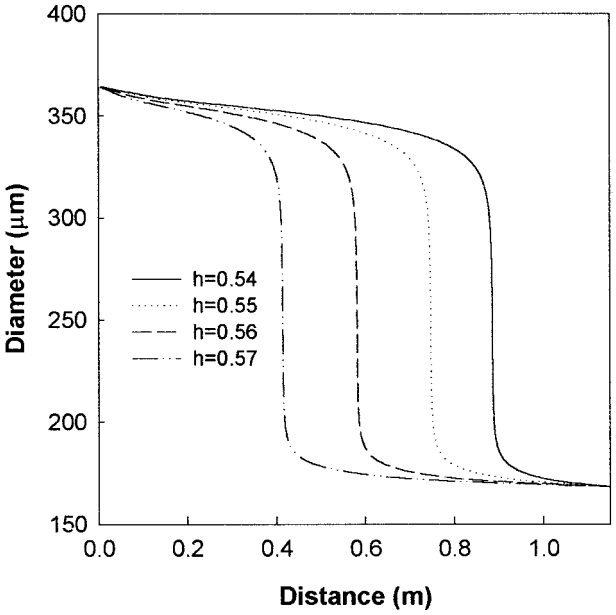

Figure 6 Effect of strain hardening on the diameter profiles in the continuous drawing.

The strain-hardening parameter, which expresses increasing resistance to further plastic stretching, was suggested to reflect the contribution of the molecular network.[2] The diameter profiles during stretching processes show a drastic reduction and subsequent stabilization as a result of the hardening effect. In continuous drawing, the initial position of stabilization shifts to the left with increasing h because the polymer hardens more rapidly, as shown in Figure 6. It is noticeable that the overall shape of the strain localization is not altered with h, different from the case of the strain-rate-sensitivity parameter. Figure 7 describes the fact that the maximum

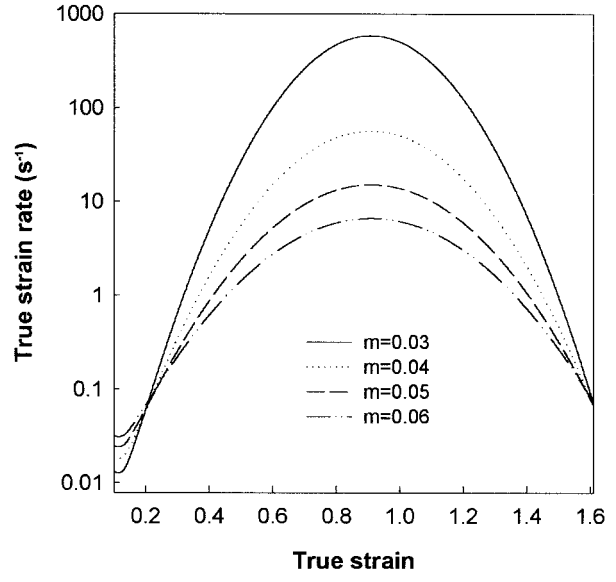

Figure 5 True strain-rate profiles as a function of true strain at various strain-rate sensitivity coefficients.

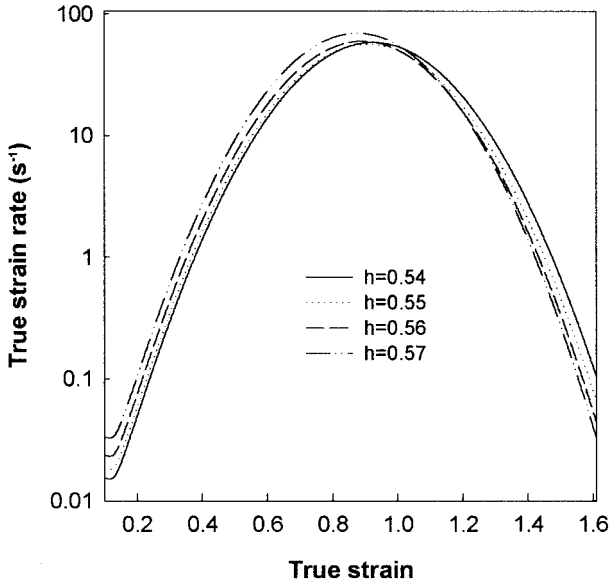

Figure 7 True strain-rate profiles as a function of true strain at various strain-hardening coefficients.

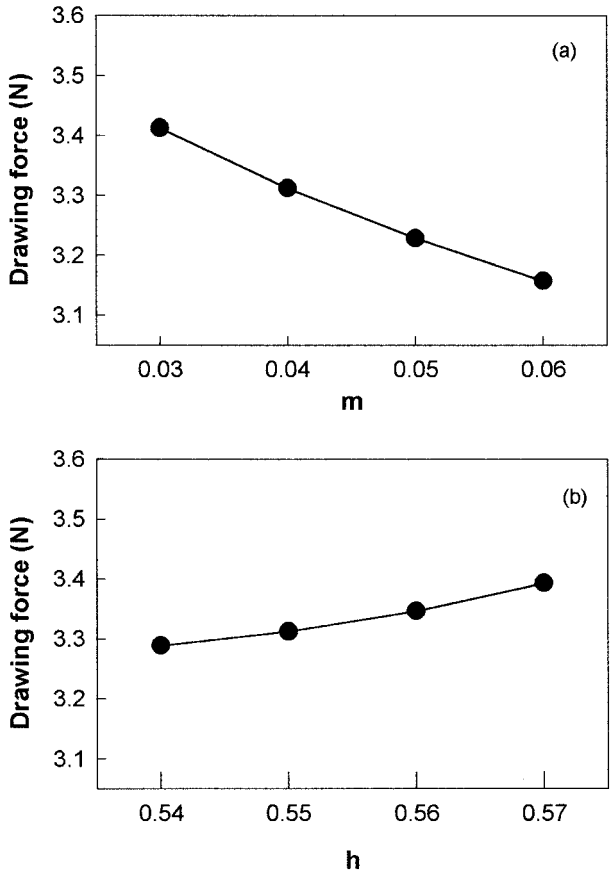

Figure 8 Effects of material parameters on the drawing force.

strain rate is almost independent of h in continuous drawing.

The drawing force, maximum strain rate, and position of the inflection point are significant variables to be considered in continuous drawing. Thus, it is of great importance to verify the effect of material parameters on these variables by the simulation since they are usually unknown in a real process.[12] The drawing force is a critical factor that influences the structural development during drawing, as is well known, and the maximum strain rate can be the index of the sharpness of the neck. Comparison of the position of the inflection point makes it possible to estimate the relative amount of region III in Figure 2, where structural development is dominant. Figure 8 describes the effects of strain-rate sensitivity and strain hardening on the drawing force which is constant along the drawing line. The increase of m results in decrease of the drawing force, meaning that the applied drawing force is small when homogeneous deformation occurs for large m. However, when the material with large h is stretched, a larger force acts on the drawing line because the material under stretching exhibits effective hardening.

Figures 9 and 10 give some insight into the overall aspects of the deformation behavior with respect to the rheological coefficients. Figure 9 shows that the position of the inflection point shifts toward the feeding roll as m and h increase. The maximum strain rate, which is a measure of the intensity of strain localization, is strongly dependent on the strain-rate sensitivity (Fig. 10), whereas the effect of strain hardening has little effect on the maximum strain rate. However, the effect of strain hardening on the position of the inflection point is more dominant than that of strain-rate sensitivity, as shown in Figure 9.

Effects of Initial Structure

The tensile behavior is sensitive to the molecular and crystalline texture of undrawn samples. The

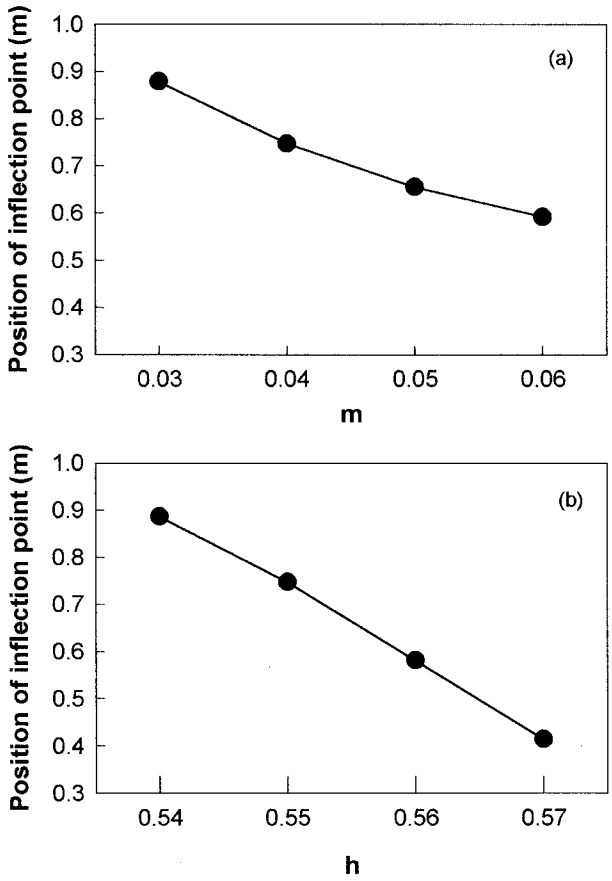

Figure 9 Effects of material parameters on the position of inflection point in the drawing line.

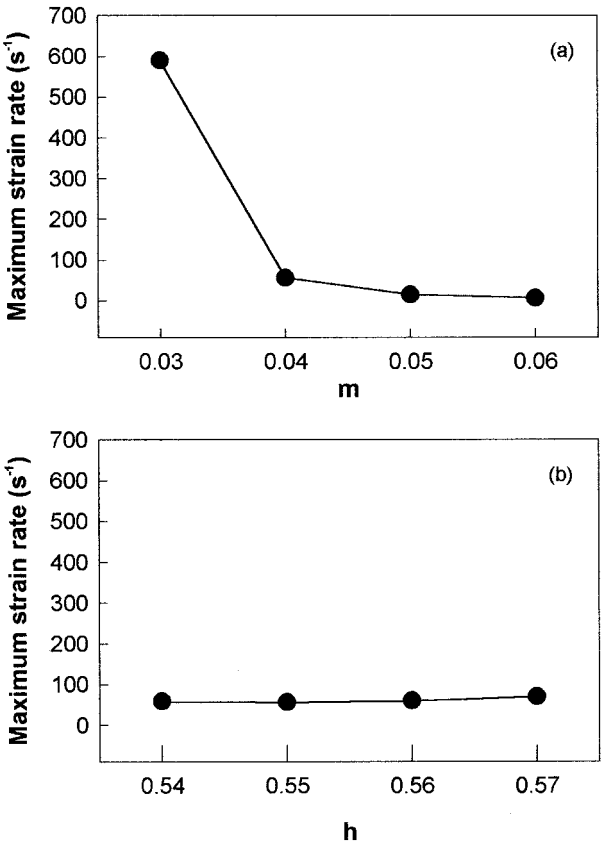

Figure 10 Effects of material parameters on the maximum strain rate in the drawing line.

dynamics of melt spinning, thus, can be a factor that influences the drawing behavior, since it determines the rheological parameters of as-spun filaments. In this study, the quenching condition during melt spinning of hollow fiber was chosen as a tool of controlling the structural parameter.

One of the important factors determining the necking behavior in cold drawing and the accompanying change in the morphology of PP hollow fibers is whether the structure of spun fibers is predominantly monoclinic or smectic.[14,15] Thus, it is important to characterize the structure of as-spun hollow fiber with regard to the spinning condition and subsequent drawing behavior. The crystalline structure, which can be commonly observed in the products of PP and in the annealed sample, is the α form, the most stable and compact one.[16–18] In the case of PP, quenching the molten polymers leads to a distinctive crystalline phase, exhibiting an order intermediate between amorphous and crystalline, the precise nature of which is still under debate. This phase has been called by various names such as smectic, paracrystalline, or condis crystal in the literature. Here, we refer to it as smectic, the most commonly used name,[19–21] which was first described by Natta and Corradini.

There have been a number of studies[16,18–21] regarding the quenching effects on the crystalline structures of PP in film specimens prepared under conditions free from stress and resultant molecular orientation. However, the melt-spinning process is accompanied by the crystallization of a strained polymer under nonisothermal conditions. Because both the rate of cooling and the tensile stress have effects on the crystallization, the crystalline phase of PP in melt spinning is not considered to coincide with that of a film specimen. Thus, for a discussion on the effects of the initial structure, it is essential to analyze the structure of PP fibers prepared with water quenching or air cooling without forced convection.

Figure 11 illustrates the equatorial WAXD intensity profiles of water-quenched PP and air-cooled PP. Two broad and diffuse diffraction pat-

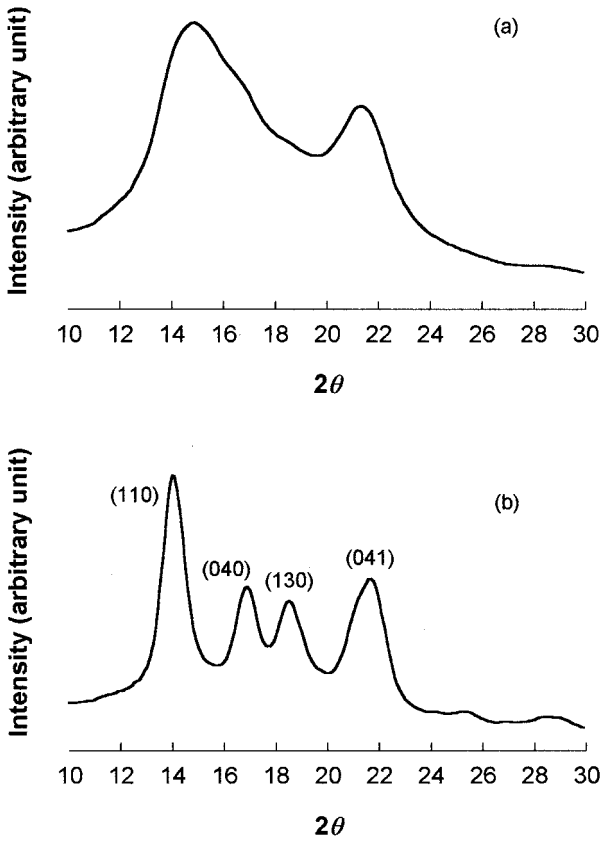

Figure 11 Equatorial WAXS patterns of undrawn PP filaments produced at different quenching conditions: (a) water-quenching; (b) air-cooling.

terns near $2\theta = 15°$ and 21° indicate that the quenched PP fibers correspond to the smectic state. From this result, it is suggested that the quenched PP is a two-phase system, that is, an amorphous and paracrystalline or smectic phase. On the other hand, the fiber spun without quenching displays typical sharp peaks of a monoclinic α form of a crystalline structure.

The DSC curves of Figure 12(a) exhibit three peaks defined as T_1, T_2, and T_3 with increasing temperature. Because the first endothermic peak (T_1) and the exothermic peak (T_2) are not clearly observed for PP fiber without quenching [Fig. 12(b)], it can be inferred that these peaks may be ascribed to a specific phase transition occurring in the quenched form of PP. T_1 is usually considered to be a melting peak of crystalline entities of small size or in a low degree of perfection, and T_2 is a well-known thermally activated process related to the exothermic process of transitions from the smectic phase to the monoclinic α form.[15,17] The thermogram of the air-cooled PP fiber displays a sharper major melting endothermic peak with small evidence of a T_1 peak. The absence of the T_2 peak in this plot indicates that the transition process found in quenched PP does not occur, and, accordingly, the fiber spun without quenching exhibits the nature of the monoclinic α form.

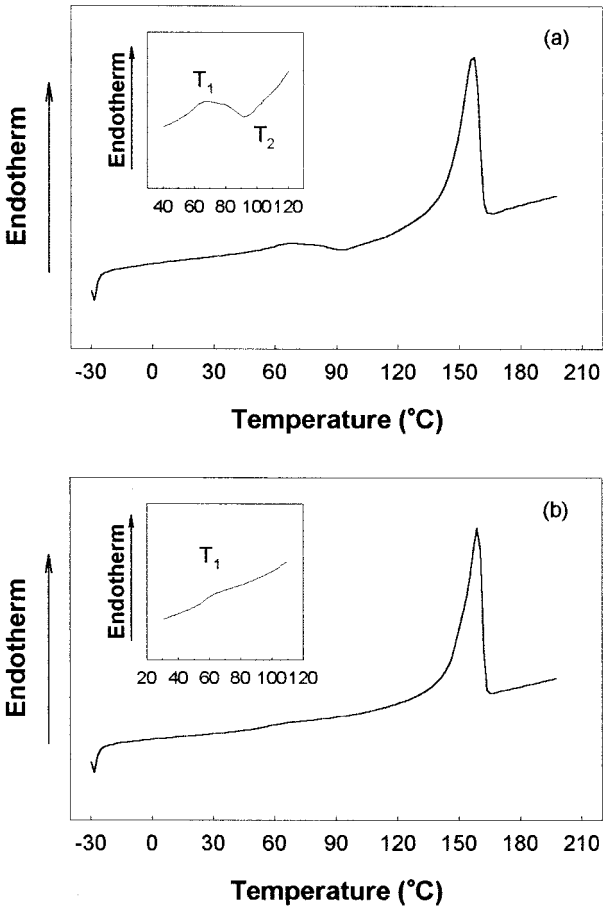

Figure 12 DSC thermograms of undrawn PP filaments produced at different quenching conditions: (a) water-quenching; (b) air-cooling. Inset: Enlargement of the thermogram near the T_1 and T_2 peaks.

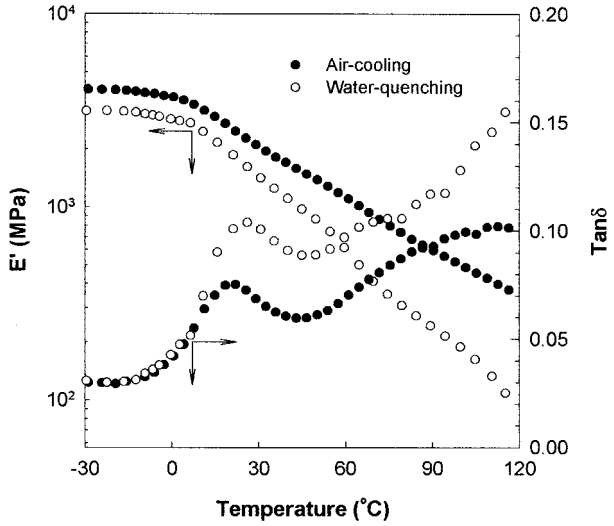

Figure 13 Storage modulus and loss factor of undrawn PP filaments produced at different quenching conditions.

Consequently, from the above structural analysis with WAXD and DSC, it can be suggested that the water-quenched PP hollow fiber has the smectic form and air-cooled PP fiber shows the monoclinic α form. This suggestion, for the structural aspects of PP hollow fiber according to quenching conditions, may again be verified by the viscoelastic behavior. The dynamic mechanical properties were measured using DMTA to obtain additional information on the microstructure of the amorphous phase and the crystalline nature. The variation of the storage modulus, E', with temperature and the loss factor, tan δ, are reported in Figure 13 for two kinds of fibers. The two E' curves show a decrease with increasing temperature as a result of the gradual activation of the molecular mobility. It is noticeable that the quenched fiber shows a steeper drop of E' than does the air-cooled fiber due to weak elastic interactions in the smectic phase. This is supported by the higher tan δ level of fiber with water quenching, which indicates greater energy absorption

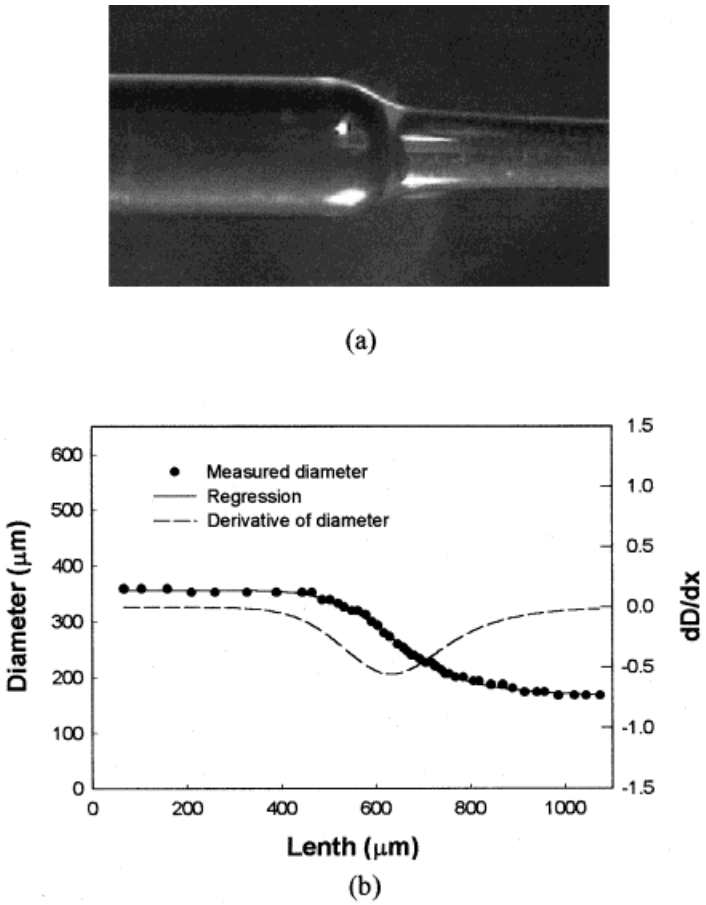

Figure 14 Necking profile and its intensity in the continuous drawing for the water-quenched PP filaments: (a) captured image of the neck; (b) regression of measured diameter profile and its derivative.

due to more intense molecular mobility in the smectic phase. Based on the above results on the structure of as-spun PP fiber, the effects of the initial crystalline structure on the necking behavior can be discussed.

The geometry of the neck was observed for the as-spun fiber with a different crystalline structure. Figures 14 and 15 illustrate that the PP hollow fibers stretched at room temperature show a sharp neck in both cases of the crystalline structure. For a quantitative description of its sharpness, the neck intensity parameter is defined as follows:

$$H = \left[\frac{dD(z)}{dz}\right]_{\max} \frac{1}{D_L - D_0} \tag{8}$$

which is analogous to the equation based on the velocity, employed in Ziabicki's work.[22] The geometrical sense of H is explained as the reciprocal length of the necking zone, so that the large value of H means intensive necking in the concentrated deformation zone. To obtain the H of each neck, the captured images were converted to continuous curves by the regression, and their derivatives were calculated numerically. From the resultant intensity of the neck, the air-cooled PP fiber, with the monoclinic α form, displays a sharper neck ($H = 5.69 \times 10^3$ m^{-1}) than that of the quenched PP fiber ($H = 3.04 \times 10^3$ m^{-1}).

The strain-rate sensitivity and the intensity of the neck can be related to the morphology of PP, as suggested by Coats and Ward, who showed the effects of the morphology on the strain-rate sensitivity of polyethylene in their article.[1] It must be recalled that the rheological parameters affect the necking behavior in the calculated results and the neck intensity is closely related to the strain-rate sensitivity, m. Following the consideration in the parametric studies of this work, the water-

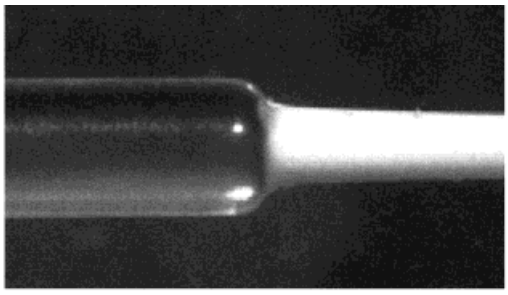

(a)

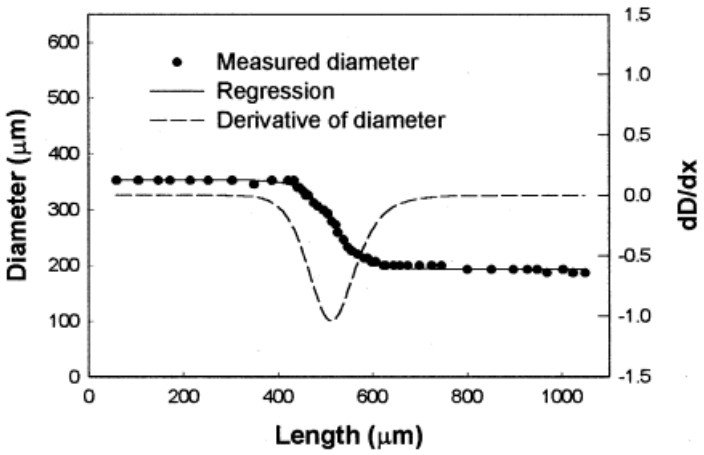

(b)

Figure 15 Necking profile and its intensity in the continuous drawing for the air-cooled PP filaments: (a) captured image of the neck; (b) regression of measured diameter profile and its derivative.

quenched PP fiber can be considered to have higher strain-rate sensitivity than that of air-cooled PP since it shows a less intensive neck. This can be explained from the structural point of view: The quenched PP fiber with the smectic form seems to exhibit a more fluidlike nature since it has less elastic interaction and a higher tan δ than that of the PP fiber with the monoclinic form as elucidated from the dynamic mechanical test. On the basis of this result, we can predict the trends of strain localization in the drawing process according to the melt-spinning condition that determines the structure of the undrawn fiber.

Figure 16 shows that the quenching condition has a significant effect on the dimension of as-spun hollow fiber. The hollowness of as-spun fiber with water quenching is larger than that without quenching. This means that the inner and outer diameters of the quenched sample are larger than are those of the nonquenched sample, due to larger hollowness of the quenched sample for the same cross-sectional area. It seems, from the results of this work and an earlier study on the spinning temperature effect, that the shorter the deformation region of the melt spinning the larger is the hollowness of as-spun fiber, that is, the shorter deformation zone due to a lower spinning temperature causes larger hollowness.[23] On the other hand, the hollowness of drawn fibers is determined by the change in the inner and outer diameters during the drawing process. As elucidated in the previous work, the hollowness of fibers drawn at 30°C, when the sharp neck can be observed, is higher than that of undrawn fibers, whereas it is lower at higher drawing temperatures. The increase in hollowness of the fibers drawn at 30°C is more remarkable for the sample without quenching, which shows a sharper neck during stretching. From the above results of the geometrical characteristics of hollow fibers, it

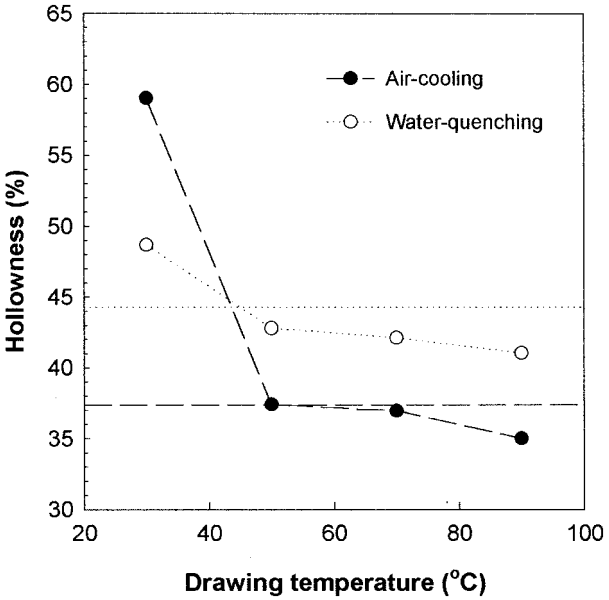

Figure 16 Hollowness of drawn fibers prepared at various drawing temperatures: (horizontal lines) hollowness of as-spun fibers: (dashed line) air-cooling; (dotted line) water-quenching.

may be inferred that the length of the deformation zone in melt spinning and the intensity of strain localization in continuous drawing are the major factors that determine the hollowness during each process.

CONCLUSIONS

It has been shown that the mathematical model, incorporated with the constitutive relation for solid polymers that can describe the true (stress–strain–strain rate) relation makes it possible to express the deformation behavior of continuous drawing. The parametric studies by the numerical method have shown that the drawing behaviors in continuous drawing are dependent on the strain-rate sensitivity and strain-hardening effects. It has also been found that the intensity of strain localization is a strong function of the strain-rate sensitivity, and strain hardening is associated mainly with the position of the inflection point. To determine the structural effects of the undrawn fiber, two distinctive initial structures of the PP fiber were formed by controlling the quenching condition in melt spinning. The filaments with a stable monoclinic phase of the crystal, prepared without quenching, were shown to be less sensitive to the strain rate and exhibited a plastic instability sharper than those with an unstable smectic phase. It was shown that different quenching conditions in melt spinning, and the resultant drawing behavior with different crystalline structures, affect the evolution of hollowness during each process.

The authors wish to acknowledge the financial support of the Korea Research Foundation made in the program year of 1998.

REFERENCES

1. Coates, P. D.; Ward, I. M. J Mater Sci 1980, 15, 2897.
2. Nazarenko, S.; Bensason, S.; Hiltner, A.; Baer, E. Polymer 1994, 35, 3883.
3. Gaucher-Miri, V.; Francois, P.; Seguela, R. J Polym Sci Polym Phys Ed 1996, 34, 1113.
4. Duffo, P.; Monasse, B.; Haudin, J. M.; G'Sell, C.; Dahoun, A. J Mater Sci 1995, 30, 701.
5. Coates, P. D.; Gibson, A. G.; Ward, I. M. J Mater Sci 1980, 15, 359.
6. Butler, R. H.; Prevorsek, D. C.; Kwon, Y. D. Polym Eng Sci 1982, 22, 329.
7. Lee, M. S.; Oh, T. H.; Kim, S. Y.; Shim, H. J. J Appl Polym Sci 1999, 74, 1836.
8. Ziabicki, A. Fundamentals of Fiber Formation; Wiley-Interscience: London, 1976.
9. Kim, J. J.; Jang, T. S.; Kwon, Y. D.; Kim, U. Y.; Kim, S. S. J Membr Sci 1994, 93, 209.
10. Kamo, J.; Hirai, T.; Takahashi, H.; Kondou, K. U.S. Patent 5 547 756, 1996.
11. Le Bourvellec, G.; Beautemps, J.; Jarry, J. P. J Appl Polym Sci 1990, 39, 319.
12. Salem, D. R. Polymer 1998, 39, 7067.
13. Haward, R. N. J Polym Sci Polym Phys Ed 1995, 33, 1481.
14. Candia, F. D.; Romano, G.; Russo, R.; Vittoria, V. Coll Polym Sci 1987, 265, 696.
15. Candia, F. D.; Russo, R.; Vittoria, V. Polym Eng Sci 1988, 28, 974.
16. Alberola, N.; Fugier, M.; Petit, D.; Fillon, B. J Mater Sci 1995, 30, 1187.
17. Poussin, L.; Bertin, Y. A.; Parisot, J.; Brassy, C. Polymer 1998, 39, 4261.
18. Seguela, R.; Staniek, E.; Escaig, B.; Fillon, B. J Appl Polym Sci 1999, 71, 1873.
19. Vittoria, V.; Perrulo, A. J Macromol Sci-Phys B 1986, 25, 267.
20. Vittoria, V. J Macromol Sci-Phys B 1989, 28, 97.
21. Vittoria, V. J Macromol Sci-Phys B 1989, 28, 489.
22. Ziabicki, A. High-Speed Fiber Spinning; Wiley-Interscience: New York, 1985, Chapter 2.
23. Oh, T. H.; Lee, M. S.; Kim, S. Y.; Shim, H. J. J Appl Polym Sci 1998, 68, 1209.